지질학회지 제 57권 제 5호, p. 691-705, (2021년 10월)
J. Geol. Soc. Korea, v. 57, no. 5, p. 691-705, (October 2021)
DOI http://dx.doi.org/10.14770/jgsk.2021.57.5.691

ISSN 0435-4036 (Print)
ISSN 2288-7377 (Online)

남극 Ross Sea 빙성해양퇴적물의 ^{10}Be과 ^{10}Be/^{9}Be: 제4기 중·후반 고환경변화에 대한 함의

Chinmay Dash[1] · 이민경[2] · 성영배[3,‡] · 이현희[3] · 이재일[2] · 유규철[2]

[1]Department of Earth Sciences, Indian Institute of Technology Roorkee
[2]극지연구소 빙하환경연구본부
[3]고려대학교 지리학과

요 약

본 연구는 남극 로스해에서 얻어진 코어(LC42)의 Be 동위원소 변화(^{10}Be, ^{9}Be, ^{10}Be/^{9}Be)를 분석하였으며 이를 제4기 고지자기와 고기후 변화의 관점에서 해석하였다. Be 동위원소는 Mid-Pleistocene Transition (MPT)를 전후로 많은 변화를 보이고 있다. ^{10}Be의 농도와 ^{10}Be/^{9}Be은 Matuyama Chron동안 점진적인 감소를 보이고 있으며, 이는 지자기강도의 상대적 증가를 지시한다. 반면에 많은 지역에서 보고된 Matuyama-Brunhes Boundary (MBB)와 관련된 ^{10}Be 과생성 사건은 본 연구에서는 발견되지 않았다. 1.0-0.8 Ma 동안에는^{10}Be과 ^{10}Be/^{9}Be은 점차적으로 감소했으며, 0.8 Ma에 최소값에 도달했다. 이는 이지역이 초기 MPT 시기 동안 상대적 open sea 환경이었으며 MIS 22에 빙하가 확장했다는 점을 시사한다. ^{10}Be과 ^{10}Be/^{9}Be은 Mid Bruhnes Event (MBE) 이전 시기에는 일정하였으며 MBE 이후 시기에는 점진적인 증가를 보이고 있다. 이는 한랭한(pre-MBE) 기후에서 온난한(post-MBE) 기후로의 전환을 지시한다.

주요어: *Be* 동위원소, 플라이스토세, 남극, 로스해, 빙하

Chinmay Dash, Min Kyung Lee, Yeong Bae Seong, Hyun Hee Rhee, Jae Il Lee and Kyu-Cheul Yoo, 2021, ^{10}Be and ^{10}Be/^{9}Be in glaciomarine sediments of Ross Sea, Antarctica: implications for mid-late Quaternary paleoenvironmental changes. Journal of the Geological Society of Korea. v. 57, no. 5, p. 691-705

ABSTRACT: This study documents the variation of *Be* isotopes (^{10}Be and ^{9}Be) and their ratio (^{10}Be/^{9}Be) from a Ross Sea sediment core (LC42) with relation to mid to late Pleistocene geomagnetic and paleoclimatic changes. Significant changes in *Be* isotope concentration are observed during pre and post-Mid-Pleistocene Transition (MPT) periods. The ^{10}Be concentration and ^{10}Be/^{9}Be ratio show a gradual decrease during the late Matuyama Chron, suggesting a relative increase in geomagnetic intensity. The overproduction episode associated with the Matuyama-Brunhes Boundary (MBB) does not show any pre- MBB precursor event. The progressively decreasing trend observed in ^{10}Be and ^{10}Be/^{9}Be ratio records from 1 to 0.8 Ma, with minimum values at around 0.8 Ma, suggests a relatively open sea condition during the early part of MPT and an extended glacial condition around MIS 22. The ^{10}Be and ^{10}Be/^{9}Be ratios are approximately constant during the pre-Mid Bruhnes Event (MBE) period and show a gradual increase after the MBE, indicating a climatic transition from colder (pre-MBE) to relatively warmer (post-MBE) conditions.

Key words: *Be* isotope, Pleistocene, Antarctica, Ross Sea, glacier

(Chinmay Dash, Department of Earth Sciences, Indian Institute of Technology Roorkee, Roorkee 247667, India; Min Kyung Lee, Jae Il Lee and Kyu-Cheul Yoo, Division of Glacial Environmental Research, Korea Polar Research Institute, Incheon 21990, Republic of Korea; Yeong Bae Seong and Hyun Hee Rhee, Department of Geography, Korea University, Seoul 02841, Republic of Korea)

‡ Corresponding author: +82-2-3290-2367, E-mail: ybseong@korea.ac.kr

1. Introduction

Interaction of primary/secondary cosmic rays with the atomic nuclei in the upper atmosphere/earth's surface produces ^{10}Be and other cosmogenic nuclides such as ^{3}He, ^{14}C, ^{21}Ne, ^{22}Ne, ^{26}Al, ^{36}Cl, and ^{53}Mn (Lal and Peters, 1967). The production of ^{10}Be usually occurs due to the spallation of Oxygen and Carbon by the cosmic ray particles. Nucleons, protons in the upper atmosphere, and neutrons at the earth's surface dominate cosmogenic nuclide production, whereas subsurface production is dominated by muons, which weakly interact with matter and retain energy for deeper penetration (Lal, 1988). Distinct processes produce two different varieties of ^{10}Be: meteoric ^{10}Be is produced in the upper atmosphere, whereas in-situ ^{10}Be is produced on Earth's surface when cosmic rays interact with oxygen atoms within the lattices of mineral grains (Quartz) (Lal and Peters, 1967). The meteoric ^{10}Be concentration in sediments has wider applicability for numerous geophysical and geochemical studies due to its high sensitivity to earth surface processes and its application to quartz free lithologies (Willenbring and von Blanckenburg, 2010). Meteoric ^{10}Be is a potential tool for estimating basin-wide erosion rate (von Blanckenburg *et al*., 2012), reconstructing paleo-secular variations of the earth's magnetic field (Aldahan and Possnert, 2003; Carcaillet *et al*., 2004; Simon *et al*., 2020), and estimating the sea-ice extent (Frank *et al*., 1995) and glacial meltwater discharge (Simon *et al*., 2016a). When normalized to its stable counterpart ^{9}Be, the ratio can circumvent the variations relating to particle size or retention behavior (von Blanckenburg *et al*., 2012) and can be applied to measure spatio-temporal variability of continental erosion rates (von Blanckenburg and Willenbring, 2014; von Blanckenburg *et al*., 2015) and record deep ocean circulation patterns (von Blanckenburg *et al*., 1996). Due to the long half-life of ^{10}Be (1.39×10^{6} yr), this ratio can be applied to study ice sheet melting dynamics for more extended periods than could be achieved using other traditional particle reactive radioisotopes ($t_{1/2}$ ^{230}Th = 7.5×10^{4} yr and $t_{1/2}$ ^{231}Pa = 3.2×10^{4} yr).

At present, there exist only a few works concerning the ^{10}Be in Antarctic sediments. Frank *et al*. (1995) studied sediment redistribution and paleo-productivity changes in the Weddell Sea sediment record and documented an increase in ^{10}Be concentration during the late Quaternary interglacials. In another study, Frank *et al*. (2002) studied quasi-conservative behavior of dissolved ^{10}Be from depth profiles of Antarctic seawater and suggested that the ^{10}Be concentrations in deeper water are less affected by the scavenging process or ice melt. Other similar studies around the Antarctic used *Be* isotopes to distinguish glacial/post-glacial sediment sources (Sjunneskog *et al*., 2007; Yokoyama *et al*., 2016), estimate variations in sea ice cover, and study amplitude and rhythm of geomagnetic field change (Raisbeck *et al*., 2006). Despite previous high-resolution studies, the present understanding of the variability of *Be* isotope concentrations in Antarctic sediments concerning paleoenvironmental changes has remained unclear, as the complex characteristics of glacial and glacio-marine sediments do not offer an uncomplicated interpretation of climatic or chronological signals (Sjunneskog *et al*., 2007). Although *Be* isotopes are subject to reworking but have different pathways than other cosmogenic radioisotopes (e.g., ^{14}C) (Willenbring and von Blanckenburg, 2010), hence can compensate for uncertainties associated with chronology and can illustrate changes in earth surface processes.

In the present study, we analyze ^{10}Be (meteoric), ^{9}Be, and their ratio from a Ross Sea sediment core to enhance our previous understanding of paleoclimatic records from Antarctic continental shelf sediments. The prime focus of this study is to analyze the applicability of *Be* isotopes as a proxy

to reconstruct Antarctic Ice sheet melting by pulsed warming intervals during mid to late Quaternary and to study the variation of ^{10}Be flux during the geomagnetic reversals.

Ross Ice Shelf occupies a large part of the Ross Sea embayment, fed by eastern glaciers and western ice streams (Sjunneskog *et al*., 2007). Together with sea ice, the ice shelf controls the ocean water circulation in decadal to millennial time scales, e.g., the ice shelf exceeded the continental shelf region during the Last Glacial Maxima (Domack *et al*., 1999; Ship *et al*., 1999), and its retreat during the post-glacial warm period resulted in renewed exposure to open ocean conditions (Sjunneskog *et al*., 2007; Jeong *et al*., 2018). As a consequence of the advance/retreat of the Antarctic ice shelf during glacial/interglacial periods, depositional environments in the Ross Sea have altered. Unlike the meteoric ^{10}Be, the ^{9}Be is primarily terrestrially sourced. Hence the *Be* isotope ratio variability in glaciomarine sequences will depend on (1) atmospheric flux, (2) sediment pathways and settling time, and (3) syn-depositional reworking. These Antarctic shelf sediment pathways are subject to change during different climactic episodes, thus proving them as a tracer to study climate-induced glaciomarine sediment dynamics.

2. Study area

The Ross Sea is an important aspect of global thermohaline circulation as it is one of the three primary sources of Antarctic Bottom Water (AABW). Flowing into the abyssal ocean, it provides cooling and ventilation of the deep ocean (Orsi *et al*., 2001). Jacobs *et al*. (2011) suggests that the AABW in the Ross Sea has recently freshened due to melt water influx from Amundsen and Bellingshausen Seas. Recent studies have suggested that upwelling of Circumpolar Deep Water (CDW) have accelerated the ice melting in the Ross Sea (Pritchard *et al*., 2012; Thompson *et al*., 2018), as it is relatively warmer (>0℃).

The Ross Sea contains the most abundant ice volume, which drains the East Antarctic Ice Sheet (EAIS) and the West Antarctic Ice Sheet (WAIS) to the Ross Ice Shelf (RIS; Fig. 1a). The RIS advanced northward during the Last Glacial Maximum (LGM), covering most of the continental shelf of the Ross Sea with glacial sediments (Anderson *et al*., 2014). The Joides Trough, which is on the outermost area of the continental shelf, was the major ice drainage of EAIS, which transported glacial sediments during the LGM (Fig. 1b) (Anderson and Bartek, 1992; Ship *et al*., 1999; Harris *et al*., 2001; Livingstone *et al*., 2012; Anderson *et al*., 2014; Halberstadt *et al*., 2016; Park *et al*., 2018). The glacial geomorphological features collected from the seafloors indicate that the Joides Trough was the front of the grounding line, and nearby Mawson and Pennell Bank show pre-LGM ^{14}C datings of carbonates (Taviani *et al*., 1993; Ship *et al*., 1999; Anderson *et al*., 2014).

The Central Basin is just in front of the Joides Trough, where the glaciomarine process could not affect during the glacial periods, and we expect the pure sea ice variance performance between the permanent sea ice coverage or seasonally opened. The basin is surrounded by the Hallett Ridge (W), abrupt gradient change from the Joides Trough (S), Iselin Bank (E), and the mouth to the Southern Ocean (N) (Fig. 1c).

3. Methods

We acquired sediment core from the Central Basin during the 2015 R/V ARAON cruise of the Korea Polar Research Institute (KOPRI). We collected the RS15-LC42 in 2084 m depth (length: 11.75 m; 71° 49.40′ S, 178° 34.76′ E), and the magnetic polarity of this core exhibited normal-to-reversed magnetism at 8.26 ± 0.03 m (0.781 Ma) (Ohneiser *et al*., 2019). Assuming constant sedimentation rate and the top sample as of modern age, the age of

the core was linearly determined using the geomagnetic reversal marker (Ohneiser *et al*., 2019).

The lithostratigraphy of the core was described in detail by Ohneiser *et al*. (2019). We followed the physical and chemical treatment procedures outlined by the Korea University Geochronology Laboratory, Seoul, to extract and measure meteoric ^{10}Be from the clay rich marine sediments (Bourles *et al*., 1989; Jeong *et al*., 2018).

A total of 55 samples were taken for beryllium isotope analyses, roughly at every 30 cm. The samples were dried and grinded for homogenization. Over 200 μm fraction was separated, and only the <200 μm fraction was selected to remove size dependency related to chemical adsorption of beryllium isotope. After oxidization for removing organic materials, 0.4 mg of ^{9}Be carrier (~1000 ppm) was added to 0.5 g of sediment samples

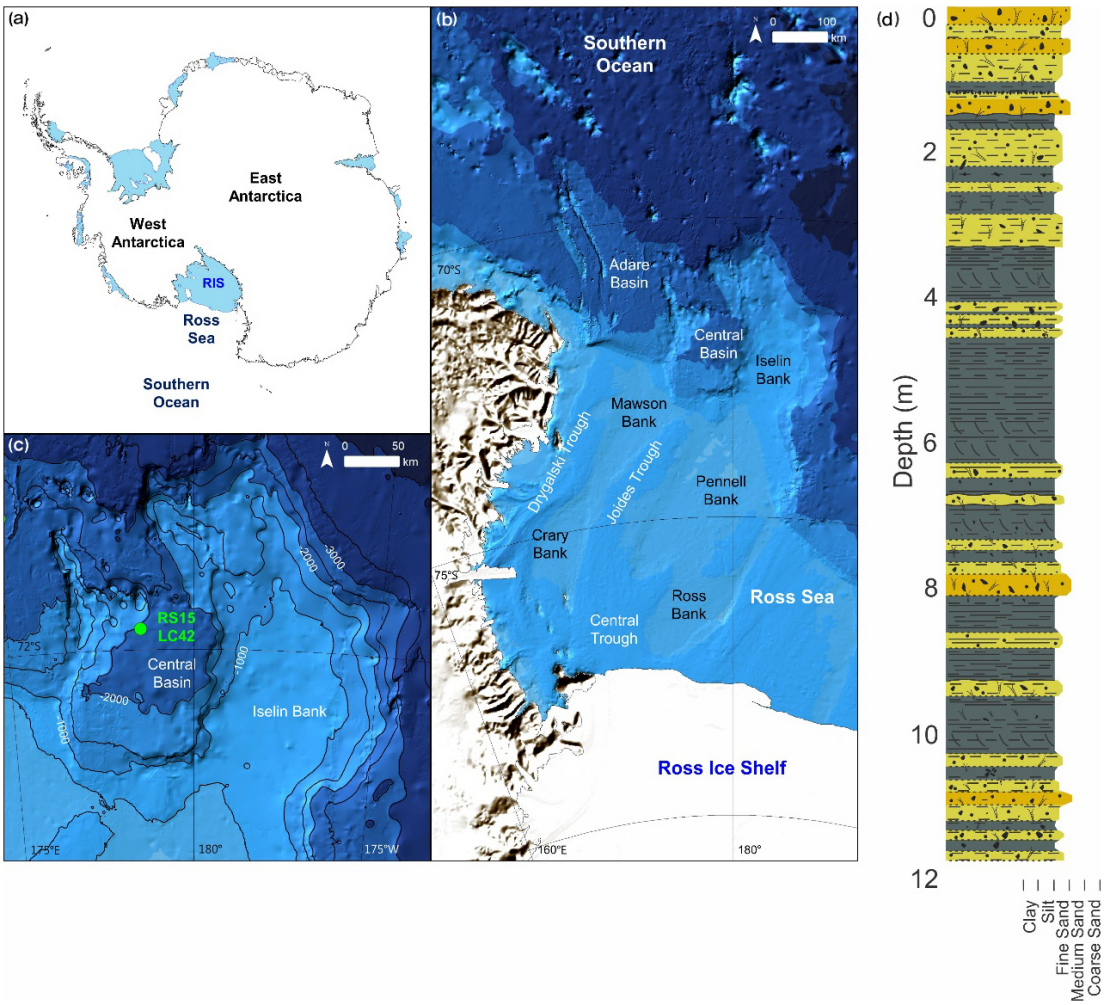

Fig. 1. Study area. (a) Map showing the location of Ross Sea, Weddell Sea, Ross Ice Shelf (RIS), East and West Antarctic Ice Sheet (b) Detailed physiographic map of Ross Sea (c) Bathymetry (in meters) map of Ross Sea showing the location of LC42 core (d) Lithostratigraphy of LC42 (Adapted from Ohneiser *et al*., 2019). Ohneiser *et al*. (2019) classified the LC42 core into three lithologically distinct units: Unit I (0-1.55 m) is dominated by gravelly muddy sand with interbeds of fine to medium sand and silt; Unit II (1.55-3.15 m) comprising of gravelly muddy sand, with interbeds of laminated and bioturbated silt; Unit III (3.15-11.78 m) consisting of clast free interbeds of laminated, sandy silt, bioturbated silt and gravelly muddy sands.

before beryllium extraction procedures. The ^{10}Be was extracted through a step-wise leaching procedure using a 0.04 M hydroxylamine in 25% acetic acid solution (Bourles *et al*., 1989), and its ^{9}Be concentration was measured by Inductively Coupled Plasma Atomic Emission Spectrometry (ICP-AES) and Mass Spectrometry (ICP-MS) at Korea Basic Science Institute (KBSI). The relative error (of 1 standard deviation) for ^{9}Be measurement is <±2.5%. ^{10}Be analyses were performed using 6 MV AMS at the Korea Institute of Science and Technology (KIST) (Lee *et al*., 2011; Rhee *et al*., 2017). The blank for the beryllium carrier averaged is less than 6.5×10^{-15}.

4. Results

The meteoric ^{10}Be and ^{9}Be data for the core taken from the Ross Sea (LC42) is shown in Table 1. The ^{10}Be concentration (Decay corrected) varies from $5.29\pm0.05\times10^{8}$ to 0.214×10^{8} atoms/g, with an average value of $1.52\pm0.02\times10^{8}$ atoms/g. The ^{10}Be concentration depicts clear contrasts between different time intervals during the past 1 Ma. Between 1 to 0.8 Ma there is a steady decrease in ^{10}Be concentration (average = $1.14\pm0.02\times10^{8}$ atoms/g), which increases sharply from 0.8 to 0.7 Ma (average= $1.96\pm0.03\times10^{8}$ atoms/g). Thereafter, the ^{10}Be concentration remains approximately constant up to ~0.43 Ma, with an average value of $0.8\pm0.01\times10^{8}$ atoms/g, which is nearly half of the whole core's average value. After 0.43 Ma, the ^{10}Be concentration increases steadily, showing maximum value at the top of the core. The average value of ^{10}Be concentration during the post 0.43 Ma period is $1.85\pm0.02\times10^{8}$ atoms/g, nearly doubling the average value of the preceding interval. The ^{9}Be concentration does not show much fluctuation throughout the core. The relative variation of average ^{9}Be concentration during these time intervals is within 10% of the average value of the core ($2.01\pm0.03\times10^{16}$ atoms/g), except an anomalously higher value corresponding to 451 cm depth (Age: 425 Ma; ^{9}Be concentration: 11×10^{16} atoms/g). The down-core variation of the ^{10}Be/^{9}Be ratio (*Be ratio*, decay corrected) mimics the variation of ^{10}Be concentration, with an average value of $0.9\pm0.01\times10^{-8}$ for the whole core. The interval between 1 to 0.8 Ma shows a gradual decrease of the ratio (average = $0.7\pm0.01\times10^{-8}$), followed by a sharp increase (0.8-.7 Ma, average = $1\pm0.01\times10^{-8}$). The most noticeable feature of the ^{10}Be in this interval is a peak overpassing the average value of all samples. The *Be ratio* remains approximately steady till 0.43 Ma (average = 0.5×10^{-8}) and further increases towards the top of the core. The average value of *Be ratio* after 0.43 Ma ($1.25\pm0.01\times10^{-8}$) doubles the preceding interval's average value. The time since the mid-Pleistocene can be divided into several climatic episodes based on *Be* isotope data from the present study and paleoclimatic inferences drawn from previous works. The glacial (light blue)/interglacial (yellow) periods corresponding to the increase/decrease of ^{10}Be concentration are shown in Fig. 2.

5. Discussion

Although using a single geomagnetic reversal event to establish the chronology of the core may impose age uncertainties on short-term climatic events, the longer climatic divisions will remain less affected. The *Be* isotope data from the present study shows changes over sub-millennial time scales, representing the variability of geomagnetic intensity and climate change over broader time intervals (Fig. 2). Thus, the present study encompassing many sub-millennial episodes of climatic variability during the past 1 Ma will not be affected by the age uncertainties.

5.1 Relationship with paleomagnetic changes

The Late Matuyama Chron witnessed an increase in the geomagnetic field intensity with significant

Table 1. The meteoric ^{10}Be and ^{9}Be Data from the core taken from the Ross Sea (LC-42).

Depth	Sample mass [g]	Carrier conc. [ppm]	Carrie mass [g]	^{9}Be counts in sample[a] [1E16/g]	AMS ^{10}Be / ^{9}Be ratio[b] [1E-11]	^{10}Be counts in sample[b, c, d] [1E8/g]	$^{10}Be/^{9}Be$ ratio [1E-8]	Decay-corrected ^{10}Be counts in sample[b, c, d] [1E8/g]	Decay-corrected $^{10}Be/^{9}Be$ ratio [1E-8]
0	0.9805	1053.6	0.3802	1.146 ± 0.011	17.061 ± 0.009	4.792 ± 0.048	4.181 ± 0.042	4.792 ± 0.048	4.181 ± 0.042
31	1.0171	1053.6	0.3638	1.928 ± 0.019	20.177 ± 0.005	5.218 ± 0.052	2.707 ± 0.027	5.295 ± 0.053	2.747 ± 0.027
61	0.9520	1053.6	0.3658	0.849 ± 0.009	10.374 ± 0.005	2.877 ± 0.029	3.389 ± 0.034	2.961 ± 0.030	3.488 ± 0.035
91	0.9883	1053.6	0.3622	1.762 ± 0.018	7.933 ± 0.002	2.099 ± 0.021	1.191 ± 0.012	2.191 ± 0.022	1.243 ± 0.012
121	0.9843	1053.6	0.3805	1.605 ± 0.016	9.727 ± 0.003	2.714 ± 0.027	1.691 ± 0.017	2.874 ± 0.029	1.791 ± 0.018
151	0.9862	1053.6	0.3826	1.354 ± 0.014	6.555 ± 0.001	1.838 ± 0.018	1.357 ± 0.014	1.974 ± 0.020	1.458 ± 0.015
161	1.0870	1047.8	0.4268	1.758 ± 0.029	2.715 ± 0.035	0.764 ± 0.013	0.435 ± 0.007	0.825 ± 0.014	0.469 ± 0.008
171	1.1694	1047.8	0.4107	2.617 ± 0.039	3.931 ± 0.044	0.992 ± 0.015	0.379 ± 0.006	1.076 ± 0.016	0.411 ± 0.006
181	1.0605	1053.6	0.3638	1.612 ± 0.016	7.256 ± 0.001	1.794 ± 0.018	1.113 ± 0.011	1.954 ± 0.020	1.212 ± 0.012
241	1.0059	1053.6	0.3757	1.692 ± 0.017	3.213 ± 0.000	0.865 ± 0.009	0.511 ± 0.005	0.970 ± 0.010	0.573 ± 0.006
301	1.0163	1053.6	0.3707	1.744 ± 0.017	7.462 ± 0.002	1.969 ± 0.020	1.129 ± 0.011	2.269 ± 0.023	1.301 ± 0.013
321	1.1343	1047.8	0.4062	2.692 ± 0.061	1.287 ± 0.026	0.330 ± 0.008	0.123 ± 0.003	0.384 ± 0.009	0.143 ± 0.003
341	1.0574	1047.8	0.4159	2.287 ± 0.042	4.197 ± 0.064	1.184 ± 0.022	0.518 ± 0.009	1.390 ± 0.025	0.608 ± 0.011
361	0.9615	1053.6	0.3628	0.832 ± 0.009	0.926 ± 0.004	0.251 ± 0.003	0.301 ± 0.003	0.297 ± 0.003	0.357 ± 0.004
381	1.0658	1047.8	0.4236	1.000 ± 0.029	0.841 ± 0.023	0.238 ± 0.007	0.238 ± 0.007	0.285 ± 0.008	0.285 ± 0.008
401	1.0287	1047.8	0.4197	1.974 ± 0.030	3.268 ± 0.036	0.963 ± 0.014	0.488 ± 0.007	1.163 ± 0.017	0.589 ± 0.009
421	0.9733	1053.6	0.3787	1.728 ± 0.017	2.150 ± 0.002	0.602 ± 0.006	0.348 ± 0.004	0.734 ± 0.007	0.425 ± 0.004
451	0.9773	1053.6	0.3681	10.995 ± 0.110	3.304 ± 0.003	0.903 ± 0.009	0.082 ± 0.001	1.118 ± 0.011	0.102 ± 0.001
471	0.9899	1047.8	0.4190	2.166 ± 0.045	1.906 ± 0.034	0.578 ± 0.012	0.267 ± 0.006	0.722 ± 0.015	0.333 ± 0.007
491	1.0398	1047.8	0.4055	2.216 ± 0.044	2.378 ± 0.040	0.667 ± 0.013	0.301 ± 0.006	0.841 ± 0.017	0.380 ± 0.007
511	0.9716	1053.6	0.3739	1.590 ± 0.062	0.616 ± 0.023	0.168 ± 0.007	0.106 ± 0.004	0.214 ± 0.008	0.135 ± 0.005
531	1.0003	1047.8	0.4195	2.096 ± 0.040	2.406 ± 0.038	0.725 ± 0.014	0.346 ± 0.007	0.932 ± 0.018	0.445 ± 0.008
551	1.0217	1047.8	0.4236	2.036 ± 0.042	1.881 ± 0.034	0.560 ± 0.012	0.275 ± 0.006	0.726 ± 0.015	0.357 ± 0.007
571	0.9594	1053.6	0.3828	1.312 ± 0.013	2.528 ± 0.001	0.728 ± 0.007	0.555 ± 0.006	0.953 ± 0.010	0.726 ± 0.007
591	1.0905	1047.8	0.4033	1.420 ± 0.034	1.368 ± 0.029	0.363 ± 0.009	0.256 ± 0.006	0.480 ± 0.011	0.338 ± 0.008
611	1.0228	1047.8	0.4331	1.398 ± 0.025	2.263 ± 0.032	0.708 ± 0.012	0.507 ± 0.009	0.945 ± 0.017	0.676 ± 0.012
631	0.9703	1053.6	0.3666	1.388 ± 0.014	1.921 ± 0.001	0.522 ± 0.005	0.376 ± 0.004	0.703 ± 0.007	0.507 ± 0.005
661	0.9736	1053.6	0.3743	1.460 ± 0.015	1.491 ± 0.002	0.414 ± 0.004	0.283 ± 0.003	0.565 ± 0.006	0.387 ± 0.004
691	0.9134	1053.6	0.3737	1.341 ± 0.013	4.003 ± 0.001	1.184 ± 0.012	0.882 ± 0.009	1.640 ± 0.016	1.223 ± 0.012

Table 1. continued.

Depth	Sample mass [g]	Carrier conc. [ppm]	Carrie mass [g]	^{9}Be counts in sample[a] [1E16/g]	AMS ^{10}Be / ^{9}Be ratio[b] [1E-11]	^{10}Be counts in sample[b, c, d] [1E8/g]	^{10}Be/^{9}Be ratio [1E-8]	Decay-corrected ^{10}Be counts in sample[b, c, d] [1E8/g]	Decay-corrected ^{10}Be/^{9}Be ratio [1E-8]
706	1.1148	1047.8	0.4142	1.922 ± 0.033	2.350 ± 0.033	0.627 ± 0.011	0.326 ± 0.006	0.875 ± 0.015	0.455 ± 0.008
751	0.9624	1053.6	0.3719	1.383 ± 0.014	4.339 ± 0.001	1.211 ± 0.012	0.875 ± 0.009	1.726 ± 0.017	1.248 ± 0.013
811	0.9668	1053.6	0.3674	0.846 ± 0.008	5.528 ± 0.001	1.517 ± 0.015	1.792 ± 0.018	2.224 ± 0.022	2.627 ± 0.026
821	1.2858	1047.8	0.4032	4.967 ± 0.067	6.462 ± 0.058	1.457 ± 0.020	0.293 ± 0.004	2.147 ± 0.029	0.432 ± 0.006
822	1.0544	1047.8	0.4265	1.091 ± 0.016	4.204 ± 0.044	1.158 ± 0.017	1.061 ± 0.015	1.706 ± 0.025	1.564 ± 0.023
823	1.2547	1047.8	0.4098	1.675 ± 0.025	3.836 ± 0.041	0.938 ± 0.014	0.560 ± 0.008	1.383 ± 0.020	0.825 ± 0.012
824	1.0443	1047.8	0.4199	1.468 ± 0.023	3.201 ± 0.038	0.926 ± 0.015	0.631 ± 0.010	1.366 ± 0.021	0.931 ± 0.015
825	1.0109	1047.8	0.4039	1.897 ± 0.027	5.166 ± 0.050	1.480 ± 0.021	0.780 ± 0.011	2.184 ± 0.031	1.151 ± 0.016
826	1.1831	1047.8	0.4272	2.988 ± 0.053	5.320 ± 0.077	1.328 ± 0.023	0.445 ± 0.008	1.962 ± 0.035	0.656 ± 0.012
827	1.0691	1047.8	0.4198	3.429 ± 0.048	6.077 ± 0.060	1.724 ± 0.024	0.503 ± 0.007	2.547 ± 0.036	0.743 ± 0.010
828	1.0445	1047.8	0.4034	3.126 ± 0.043	5.487 ± 0.050	1.592 ± 0.022	0.509 ± 0.007	2.353 ± 0.032	0.753 ± 0.010
829	1.0294	1047.8	0.4099	1.729 ± 0.025	4.507 ± 0.046	1.333 ± 0.019	0.771 ± 0.011	1.971 ± 0.028	1.140 ± 0.016
830	0.7057	1047.8	0.4224	1.153 ± 0.018	3.357 ± 0.041	1.377 ± 0.022	1.194 ± 0.019	2.037 ± 0.032	1.767 ± 0.028
831	1.1140	1047.8	0.4213	2.483 ± 0.043	4.405 ± 0.061	1.240 ± 0.021	0.499 ± 0.009	1.835 ± 0.032	0.739 ± 0.013
832	1.1473	1047.8	0.4225	2.520 ± 0.035	5.194 ± 0.051	1.331 ± 0.019	0.528 ± 0.007	1.970 ± 0.028	0.782 ± 0.011
841	0.9500	1053.6	0.3643	1.368 ± 0.014	2.444 ± 0.001	0.677 ± 0.007	0.495 ± 0.005	1.006 ± 0.010	0.736 ± 0.007
861	1.1546	1047.8	0.4028	1.360 ± 0.039	1.133 ± 0.030	0.300 ± 0.009	0.220 ± 0.006	0.450 ± 0.013	0.331 ± 0.009
881	1.0626	1047.8	0.4353	2.509 ± 0.052	1.926 ± 0.035	0.532 ± 0.011	0.212 ± 0.004	0.806 ± 0.017	0.321 ± 0.007
901	0.9783	1053.6	0.4028	1.320 ± 0.013	1.872 ± 0.001	0.554 ± 0.006	0.420 ± 0.004	0.848 ± 0.009	0.643 ± 0.007
921	1.0165	1047.8	0.4089	2.509 ± 0.091	2.513 ± 0.087	0.745 ± 0.027	0.297 ± 0.011	1.150 ± 0.042	0.458 ± 0.017
961	0.9572	1053.6	0.3642	1.401 ± 0.014	3.557 ± 0.001	0.977 ± 0.010	0.697 ± 0.007	1.537 ± 0.015	1.097 ± 0.011
1021	0.9629	1053.6	0.3665	1.818 ± 0.018	4.863 ± 0.002	1.334 ± 0.013	0.734 ± 0.007	2.159 ± 0.022	1.188 ± 0.012
1081	0.9716	1053.6	0.3686	1.734 ± 0.017	6.710 ± 0.002	1.842 ± 0.018	1.062 ± 0.011	3.068 ± 0.031	1.769 ± 0.018
1111	0.9686	1053.6	0.3692	1.713 ± 0.017	4.688 ± 0.003	1.291 ± 0.013	0.754 ± 0.008	2.181 ± 0.022	1.273 ± 0.013
1141	0.9560	1053.6	0.3697	1.755 ± 0.001	3.310 ± 0.001	0.921 ± 0.009	0.525 ± 0.005	1.579 ± 0.016	0.900 ± 0.009
1171	0.9750	1053.6	0.3776	12.118 ± 0.127	2.080 ± 0.006	0.583 ± 0.006	0.048 ± 0.001	1.014 ± 0.011	0.084 ± 0.001

[a]Concentration of ^{9}Be was calculated from ICP-MS measured results.
[b]The ^{10}Be/^{9}Be ratios were normalized using 07KNSTD reference sample 5-1 (2.71E-11 ± 1.69E-13) of Nishiizumi *et al.* (2007) and ^{10}Be half-life of 1.38E6 (Korschinek *et al.*, 2010).
[c]Blank corrected ^{10}Be concentration (8.285E-15).
[d]Age and decay correction were calculated from paleo-magnetic reversal age at 826 cm / 0.78 Ma (Ohneiser *et al.*, 2019) and ^{10}Be half-life of 1.38E6 (Korschinek *et al.*, 2010).

peaks at around 870 ka, 910 ka, and 960 ka (Valet and Meynadier, 1993; Meynadier *et al*., 1994; Kok and Tauxe, 1999; Dinarès-Turell *et al*., 2002). These episodes of intensity maximas (spanning about

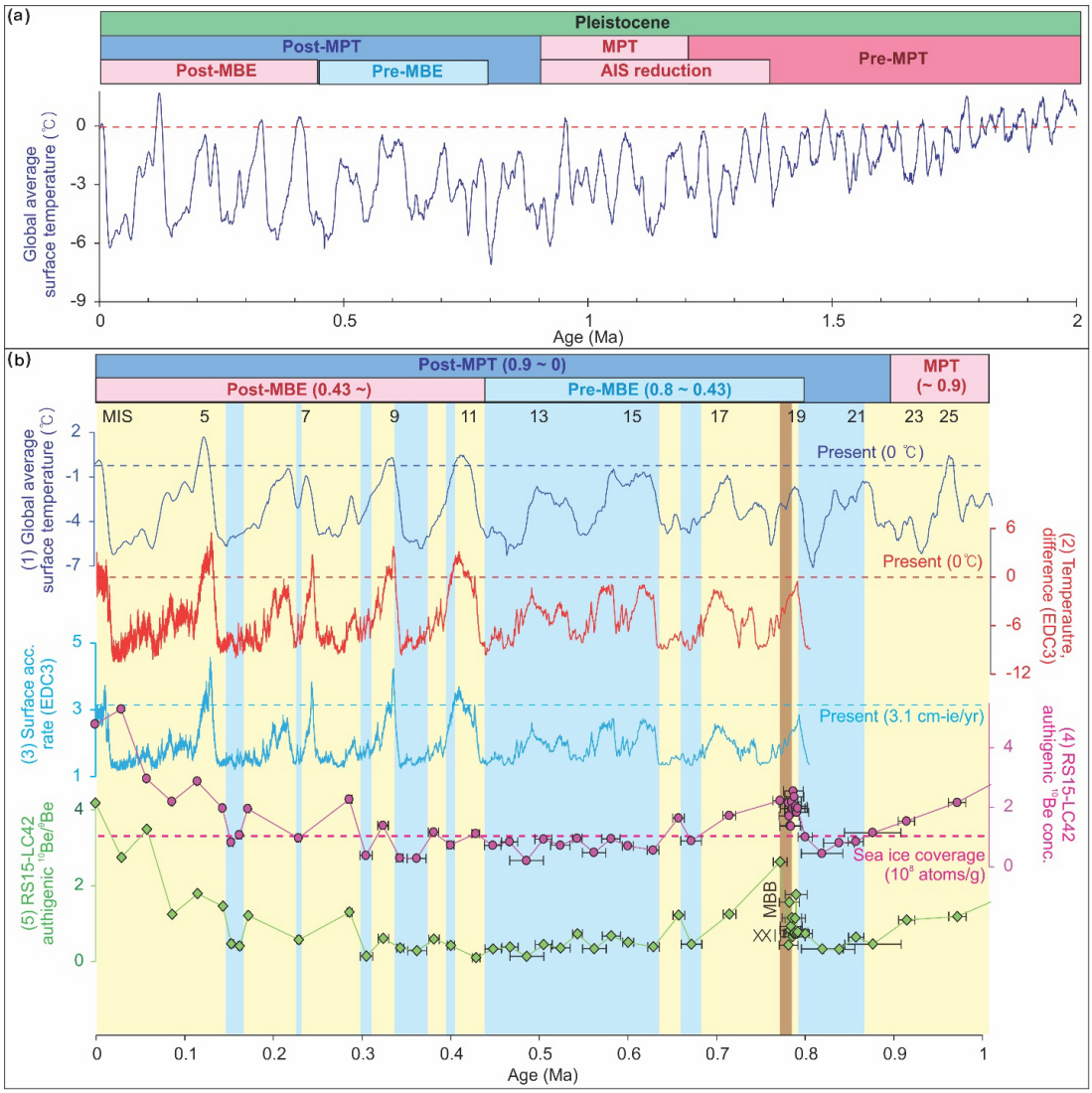

Fig. 2. (a) Global average surface temperature (GAST) changes based on deep sea oxygen isotopes over the last 2 Ma (Snyder, 2016). Our EAIS deglaciations coincide with the early Pleistocene warm period (pre-mid-Pleistocene transition, pre-MPT; 45) and the late Pleistocene warm interglacial periods (post-mid-Bruhnes transition event, post-MBE; 51, 56). (b) Climate proxy changes during the last 1 Ma. (1) GAST changes. (2) The temperature gradient between the interior EAIS temperature history (East Antarctica Dome C, EDC3; 47) and present temperature. (3) Surface accumulation rate, in centimeters of ice equivalent per year (EDC3; 57). (4) and (5) meteoric ^{10}Be concentrations and ^{10}Be/^{9}Be ratios along Long Core 42, collected during the 2015 Ross Sea cruise (this study). The sky-blue boxes represent periods of meteoric ^{10}Be depletion, which indicates more and thick sea ice coverage over the ocean surface due to a decrease in temperature that hindered the direct deposition of meteoric ^{10}Be to the seafloor. The yellow boxes indicate seasonally opened periods. The brown box represents a weakened Geomagnetic Dipole Moment (GDM, XXI) period (Matuyama- Brunhes Boundary; MBB) that is < 20% of the averaged GDM and produced higher meteoric ^{10}Be than the other periods (Simon *et al*., 2016a). The ^{10}Be peaks during the period highlighted by the brown box should be interpreted with caution.

50 ka) were separated by periods of lower intensity. The ^{10}Be and ^{10}Be/^{9}Be ratios show a gradual decrease during the late Matuyama Chron. Although the coarse sample resolution in the present study does not depict high-resolution geomagnetic changes during this period, a decreasing trend towards the Matuyama-Brunhes boundary (MBB) suggests a relative increase in paleointensity. A significant increase in the ^{10}Be and ^{10}Be/^{9}Be values is observed during 0.8-0.7 Ma. No significant correlation is found between the *Be* isotopic record and other available paleoclimatic proxies during this period, suggesting a possible paleointensity variation (Ohneiser *et al*., 2019). The *Be* overproduction episode observed during this period is synchronous with U-Pb zircon age of MBB (772.7±7.2 ka) from Byakubi-E tephra (coupled with Oxygen isotope chronology) (Suganuma *et al*., 2015), ^{10}Be overproduction observed in equatorial Pacific ocean (Simon *et al*., 2016b), the age of MBB obtained from ^{40}Ar/^{39}Ar chronology of North Atlantic marine cores (mean age of 773.1 ka) (Channell *et al*., 2010) and the peak ^{10}Be flux (during 777-766 ka) observed in EPICA (European Project for Ice Coring in Antarctica) Dome C ice core (Raisbeck *et al*., 2006). This near-doubling of ^{10}Be production during the MIS 19 resembles overproduction episodes associated with the largest geomagnetic reversals or collapse of geomagnetic dipole during long-term reversals (Raisbeck *et al*., 2006). Since there is no previous ^{10}Be overproduction episode closely associated with the MBB overproduction, our results contradict the frequently reported pre- MBB precursor event (Hartl and Tauxe, 1996; Singer *et al*., 2005; Raisbeck *et al*., 2006).

Yamazaki (1999) documented high-resolution relative paleointensity variations during the Brunhes Chron from sediment cores of the Pacific Ocean. The results showed an increase in intensity after the MBB till the Mid-Bruhnes Event (MBE) (during the pre-MBE period). In contrast, a gradual decrease in intensity is observed during the post MBE period. A significant drop in intensity was observed at about 30-50, 110-120, 180-200, 280-300, 380-410, and 520-550 ka. The *Be* isotopic records from our study agree with the relative paleointensity records from the previous studies. The ^{10}Be and ^{10}Be/^{9}Be ratios are approximately constant during the pre-MBE period and show a gradual increase after the MBE. Although the sampling resolution for the present study was high, geomagnetic reversals/excursions during the Brunhes Chron could be identified based on relative variation in the ^{10}Be and ^{10}Be/^{9}Be records (Fig. 3). *Be* overproduction episodes are observed during 25 ka (Mono Lake excursion, dated 24-39 ka by Kent *et al*. (2002)), 114 ka (Blake excursion, dated 110-120 ka by Macrì *et al*. (2005)), 171 and 284 ka (Biwa I and Biwa II, respectively, dated 187-192 ka and 292-298 ka by Worm, (1997)), 322 ka (Calabrian Ridge 1, dated at 315-325 ka by Langereis *et al*. (1997)), and 378 ka, (Levantine dated at 360-370 ka by Langereis *et al*. (1997)).

5.2 Relationship with Pleistocene climatic changes

The Mid Pleistocene Transition (MPT) started at ~1.2 Ma and ended at around 0.9 Ma, shifting gradually from warmer to colder conditions (Elderfield *et al*., 2012; Sutter *et al*., 2019). The Early to Mid-Pleistocene warmer interval is evident from the Prydz Bay sediment record, with a decreasing value of δ^{18}O and the presence of hemipelagic clay layers containing abundant planktonic/benthic species (indicative of open sea condition) (Theissen *et al*., 2003). The climate index approach of Sutter *et al*. (2019) show colder conditions towards the end of MPT, forming marine ice sheets in Weddell and the Ross Sea and prolonged glacial conditions between marine isotope stages (MIS) 25 and 22 (0.94-0.88 Ma BP). Elderfield *et al*. (2012) showed an abrupt increase in the ice sheet volume at the onset of MIS 22. The anomalously low southern hemisphere summer insolation suppressed the melting during the MIS

23, which renewed the ice growth during MIS 22. The progressively decreasing trend observed in ^{10}Be and ^{10}Be/^{9}Be ratio records from 1 to 0.8 Ma with minimum values at around 0.8 Ma corroborates previous findings of a relatively open sea condition during the early part of MPT and an extended glacial condition around MIS 22. The warmer early-MPT period is also evident from Cape Roberts Project drilling in McMurdo Sound, with enriched biogenic carbonate-rich deposits during 1 Ma BP, overlying the older glacial deposits. (Taviani and Claps, 1998) Although the relative paleointensity at MBB reduced significantly to facilitate the overproduction of ^{10}Be, the seasonal opening of Ross sea during warmer MIS 19 can be considered as another dominant contributing factor for the overproduction (Jouzel *et al*., 2007).

The past 0.8 Ma witnessed a dominant 100 Ka glacial-interglacial climatic cyclicity (Imbrie *et al*., 1993; Mudelsee and Schulz, 1997; Elderfield *et al*., 2012; Barth *et al*., 2018). The Milankovitch cycle shifted from 41 ka to 100 ka, causing significant temperature variations, albeit under cold conditions (post-MPT). The increase in the amplitude of 100 Ka cycles across the MBE is related to the change in earth's eccentricity and precession. The colder conditions persisted till 430 ka (Yin, 2013), and short interglacials punctuated the extended glacial periods during this period. The interglacial periods became relatively warmer across the MIS 11 (after 430 Ka BP, MIS 1, 5, 9, and 11) (Jouzel *et al*., 2007; Yin and Berger, 2010), with higher atmospheric CO_2 concentration (Barker *et al*., 2006; Lüthi *et al*., 2008). This climatic transition across the 430 Ka boundary is sometimes referred to as Mid-Bruhnes Transition. Pre-MBE (0.8-0.43 Ma) witnessed reduced temperature, which not only triggered the northern ice sheet growth (Snyder, 2016) but also increased the formation of the Antarctic bottom water with colder deep ocean water (Yin, 2013). The Ross Sea was seasonally open during the post-MBE warmer period, with less ice cover in vertical and lateral extent than the pre-MBE period. Our results showing high ^{10}Be production after 430 Ka also suggest post-MBE interglacials (MIS 1, 5, 9, and 11) were relatively warmer than that of the pre-MBE period (MIS 13, 15, and 17). As there is a

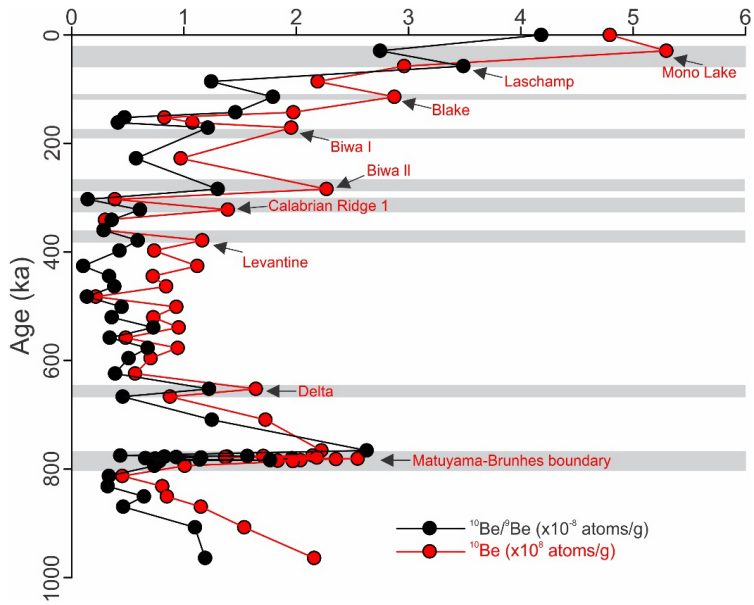

Fig. 3. Relative variation of ^{10}Be concentration and ^{10}Be/^{9}Be ratio during different geomagnetic reversals/excursions.

clear transition of the *Be* isotopic data between pre and post MBE period, the age of MBE in the present study can be recognized as another marker age for the core.

Ohneiser *et al*. (2019) compared the magnetic mineralogy of the near shelf (cores: RS15-LC42 and RS15-LC47)) and abyssal plain (cores: RS15-LC48 and RS15-LC108) sediments of Ross Sea. The inner shelf cores exhibited lower coercivity and coarser mineral magnetic population as compared to the abyssal plain sediments. The central basin is in close proximity to sources of glacial sediment with ice rafting, and gravity flows as the dominant processes of sediment supply, which get remobilized by bottom water currents (Meyers, 1982; Ehrmann, 1998; Howe *et al*., 1998; Domack *et al*., 1999; Anderson *et al*., 2014; Halberstadt *et al*., 2016). RS15-LC42 is located near the continental margin, in the flow path of high-energy cold, dense shelf waters, making a favorable condition for the deposition of coarser magnetic grains. The finer magnetic grains are carried further northward into the abyssal plain environment. The coarser sand beds along with gravel size inter-clasts and devoid of any depositional structures were indeed deposited by ice rafting, and further winnowed by strong bottom water currents (Fig. 1d) (Gilbert *et al*., 1998). In contrast, fine-grained interbeds with few local laminations suggest deposition under weaker bottom currents. Thus, alteration of poorly sorted sand and unsorted mud deposits can be attributed to temporal changes in sediment supply corresponding to changes in strength of bottom water circulation. Correlation of lithostratigraphy with climatic inferences from *Be* isotopic record of this study shows that relatively coarser sediments were deposited during the warmer climatic intervals and *vice versa*. Gravelly muddy sand deposits with presence of clasts at bottom of the core corroborates with relatively warmer conditions during early part of MPT. A short interval of coarse sediment deposition is observed around 8 m depth, corresponding to MBB. Although *Be* overproduction episode at MBB is associated with geomagnetic reversal, the coarser sedimentation suggests a short interglacial period with strengthened bottom water circulation. Progressively coarser sedimentation towards the top of the core suggests extensive deglaciation during late Quaternary period and is consistent with the gradual increase in ^{10}Be values after MBE. Textural studies of Weddell Sea sediments suggest strengthening/weakening of bottom currents during interglacial/glacial periods, respectively (Melles, 1992; Pudsey, 1992). Bottom-current at the coring site is primarily driven by Ross Sea Bottom Water (RSBW) production. The fine-grained deposits in the inner shelf area imply intermittent reduction in RSBW production and, hence, expansion of shelf ice. We conclude that coarse-grained units in the lithostratigraphy were deposited under strengthened bottom current conditions in a relatively warm climate (interglacial), and finer units reflect weak bottom currents in a cooler climate (glacial).

6. Conclusions

The ^{10}Be concentration in the Antarctic open marine condition is about 1.5×10^{9} atoms/g (Sjunneskog *et al*., 2007). However, the LC42 record exhibit concentration of a magnitude of less than one degree throughout the core. The concluding points from the present study are:

1) The downcore variation of the ^{10}Be and $^{10}Be/^{9}Be$ in the Ross Sea sediment core illustrates glacial-interglacial transitions during the mid to late Pleistocene period. The relatively high/low concentration of ^{10}Be indicates relatively open marine/sea ice-dominated conditions, respectively.

2) The gradual decrease in the ^{10}Be concentration from 1 to 0.8 Ma suggests relatively extended glacial conditions persisted during the late Matuyama Chron. This study shows that the MIS 22 was the

coldest period during the late Matuyama Chron, which corroborates previous studies showing an abrupt increase in the ice sheet volume at the onset of MIS 22. The progressively increasing trend observed in the ^{10}Be concentration after 430 Ka suggests that the post-MBE period was relatively warmer than the pre-MBE period.

3) The downcore variation of the ^{10}Be and ^{10}Be/^{9}Be ratio shows some degree of correlation with the geomagnetic reversals/excursions. No precursor event associated with the MBB reversal contradicts previous investigations showing a pre-MBB overproduction episode closely associated with the MBB overproduction episode.

4) This study shows that further investigations in marginal environments of RIS may be useful to document high-resolution glacial-interglacial transitions, as sediment characteristics at this boundary between the ice shelf and open marine environment is sensitive to small changes in the amplitudes of climate cyclicity.

Acknowledgments

This research was supported by Korea Polar Research Institute (PE21090).

REFERENCES

Aldahan, A. and Possnert, G., 2003, Geomagnetic and climatic variability reflected by ^{10}Be during the Quaternary and late Pliocene. Geophysical research letters, 30, https://doi.org/10.1029/2002GL016077.

Anderson, J.B. and Bartek, L.R., 1992, Cenozoic glacial history of the Ross Sea revealed by intermediate resolution seismic reflection data combined with drill site information. The Antarctic Paleoenvironment: A Perspective on Global Change: Part One, 56, 231-264.

Anderson, J.B., Conway, H., Bart, P.J., Witus, A.E., Greenwood, S.L., McKay, R.M., Hall, B.L., Ackert, R.P., Licht, K., Jakobsson, M. and Stone, J.O., 2014, Ross Sea paleo-ice sheet drainage and deglacial history during and since the LGM. Quaternary Science Reviews, 100, 31-54.

Barker, S., Archer, D., Booth, L., Elderfield, H., Henderiks, J. and Rickaby, R.E.M., 2006, Globally increased pelagic carbonate production during the Mid-Brunhes dissolution interval and the CO_2 paradox of MIS 11. Quaternary Science Reviews, 25, 3278-3293.

Barth, A.M., Clark, P.U., Bill, N.S., He, F. and Pisias, N.G., 2018, Climate evolution across the mid-brunhes transition. Climate of the Past, 14, 2071-2087.

Bourles, D., Raisbeck, G.M. and Yiou, F., 1989, ^{10}Be and ^{9}Be in marine sediments and their potential for dating. Geochimica et Cosmochimica Acta, 53, 443-452.

Carcaillet, J., Bourlès, D., Thouveny, N. and Arnold, M., 2004, A high resolution authigenic ^{10}Be/^{9}Be record of geomagnetic moment variations over the last 300 ka from sedimentary cores of the Portuguese margin. Earth and Planetary Science Letters, 219, 397-412.

Channell, J.E.T., Hodell, D.A., Singer, B.S. and Xuan, C., 2010, Reconciling astrochronological and ^{40}Ar/^{39}Ar ages for the Matuyama-Brunhes boundary and late Matuyama Chron. Geochemistry, Geophysics, Geosystems, 11, https://doi.org/10.1029/2010GC003203.

Dinarès-Turell, J., Sagnotti, L. and Roberts, A.P., 2002, Relative geomagnetic paleointensity from the Jaramillo Subchron to the Matuyama/Brunhes boundary as recorded in a Mediterranean piston core. Earth and Planetary Science Letters, 194, 327-341.

Domack, E.W., Jacobson, E.A., Shipp, S. and Anderson, J.B., 1999, Late Pleistocene-Holocene retreat of the West Antarctic Ice-Sheet system in the Ross Sea: Part 2-sedimentologic and stratigraphic signature. Geological Society of America Bulletin, 111, 1517-1536.

Ehrmann, W., 1998, Implications of late Eocene to early Miocene clay mineral assemblages in McMurdo Sound (Ross Sea, Antarctica) on paleoclimate and ice dynamics. Palaeogeography, Palaeoclimatology, Palaeoecology, 139, 213-231.

Elderfield, H., Ferretti, P., Greaves, M., Crowhurst, S., McCave, I.N., Hodell, D. and Piotrowski, A.M., 2012, Evolution of ocean temperature and ice volume through the mid-Pleistocene climate transition. Science, 337, 704-709.

Frank, M., Eisenhauer, A., Bonn, W.J., Walter, P., Grobe, H., Kubik, P.W., Dittrich-Hannen, B. and Mangini, A., 1995, Sediment redistribution versus paleoproductivity change: Weddell Sea margin sediment stratigraphy and biogenic particle flux of the last 250,000 years deduced from ^{230}Th$_{ex}$, ^{10}Be and biogenic barium profiles. Earth and Planetary Science Letters, 136, 559-573.

Frank, M., van der Loeff, M.M.R., Kubik, P.W. and Mangini, A., 2002, Quasi-conservative behaviour of ^{10}Be in deep waters of the Weddell Sea and the Atlantic sector of the Antarctic Circumpolar Current. Earth and Planetary Science Letters, 201, 171-186.

Gilbert, I.M., Pudsey, C.J. and Murray, J.W., 1998, A sediment record of cyclic bottom-current variability from the northwest Weddell Sea. Sedimentary geology, 115, 185-214.

Halberstadt, A.R.W., Simkins, L.M., Greenwood, S.L. and Anderson, J.B., 2016, Past ice-sheet behaviour: retreat scenarios and changing controls in the Ross Sea, Antarctica. The Cryosphere, 10, 1003-1020.

Harris, P.T., Brancolini, G., Armand, L., Busetti, M., Beaman, R.J., Giorgetti, G., Presti, M. and Trincardi, F., 2001, Continental shelf drift deposit indicates non-steady state Antarctic bottom water production in the Holocene. Marine Geology, 179, 1-8.

Hartl, P. and Tauxe, L., 1996, A precursor to the Matuyama/Brunhes transition-field instability as recorded in pelagic sediments. Earth and Planetary Science Letters, 138, 121-135.

Howe, J., Woolfe, K. and Fielding, C.R., 1998, Lower Miocene glacimarine gravity flows, Cape Roberts Drillhole-1, Ross Sea, Antarctica. Terra Antartica, 5, 393-399.

Imbrie, J., Berger, A., Boyle, E.A., Clemens, S.C., Duffy, A., Howard, W.R., Kukla, G., Kutzbach, J., Martinson, D.G., McIntyre, A., Mix, A.C., Molfino, B., Morley, J.J., Peterson, L.C., Pisias, N.G., Prell, W.L., Raymo, M.E., Shackleton, N.J. and Toggweiler, J.R., 1993, On the structure and origin of major glaciation cycles 2. The 100,000-year cycle. Paleoceanography, 8, 699-735.

Jacobs, S.S., Jenkins, A., Giulivi, C.F. and Dutrieux, P., 2011, Stronger ocean circulation and increased melting under Pine Island Glacier ice shelf. Nature Geoscience, 4, 519-523.

Jeong, A., Lee, J.I., Seong, Y.B., Balco, G., Yoo, K.-C., Yoon, H.I., Domack, E., Rhee, H.H. and Yu, B.Y., 2018, Late Quaternary deglacial history across the Larsen B embayment, Antarctica. Quaternary Science Reviews, 189, 134-148.

Jouzel, J., Masson-Delmotte, V., Cattani, O., Dreyfus, G., Falourd, S., Hoffmann, G., Minster, B., Nouet, J., Barnola, J.-M. and Chappellaz, J., *et al*., 2017, Orbital and millennial Antarctic climate variability over the past 800,000 years. Science, 317, 793-796.

Kent, D.V., Hemming, S.R. and Turrin, B.D., 2002, Laschamp excursion at Mono lake?. Earth and Planetary Science Letters, 197, 151-164.

Kok, Y.S. and Tauxe, L., 1999, A relative geomagnetic paleointensity stack from Ontong-Java Plateau sediments for the Matuyama. Journal of Geophysical Research: Solid Earth, 104, 25401-25413.

Korschinek, G., Bergmaier, A., Faestermann, T., Gerstmann, U.C., Knie, K., Rugel, G., Wallner, A., Dillmann, I., Dollinger, G., Lierse von Gostomski, Ch., Kossert, K., Maiti, M., Poutivtsev, M. and Remmert, A., 2010, A new value for the half-life of ^{10}Be by heavy-ion elastic recoil detection and liquid scintillation counting. Nuclear Instruments and Methods in Physics Research Section B: Beam Interactions with Materials and Atoms, 268, 187-191.

Lal, D., 1988, In situ-produced cosmogenic isotopes in terrestrial rocks. Annual Review of Earth and Planetary Sciences, 16, 355-388.

Lal, D. and Peters, B., 1967, Cosmic ray produced radioactivity on the Earth. In: Kosmische Strahlung II/Cosmic Rays II. Springer, 551-612.

Langereis, C.G., Dekkers, M.J., de Lange, G.J., Paterne, M. and van Santvoort, P.J.M., 1997, Magnetostratigraphy and astronomical calibration of the last 1.1 Myr from an eastern Mediterranean piston core and dating of short events in the Brunhes. Geophysical Journal International, 129, 75-94.

Lee, S.Y., Seong, Y.B., Shin, Y.-K., Choi, K.H., Kang, H.-C. and Choi, J.-H., 2011, Cosmogenic ^{10}Be and OSL dating of fluvial strath terraces along the Osip-Cheon river, Korea: tectonic implications. Geosciences Journal, 15, 359-378.

Livingstone, S.J., Cofaigh, C.Ó., Stokes, C.R., Hillenbrand, C.-D., Vieli, A. and Jamieson, S.S.R., 2012, Antarctic palaeo-ice streams. Earth-Science Reviews, 111, 90-128.

Lüthi, D., Le Floch, M., Bereiter, B., Blunier, T., Barnola, J.-M., Siegenthaler, U., Raynaud, D., Jouzel, J., Fischer, H., Kawamura, K. and Stocker, T.F., 2008, High-resolution carbon dioxide concentration record 650,000-800,000 years before present. Nature, 453, 379-382.

Macrì, P., Sagnotti, L., Dinarès-Turell, J. and Caburlotto, A., 2005, A composite record of Late Pleistocene relative geomagnetic paleointensity from the Wilkes Land Basin (Antarctica). Physics of the Earth and Planetary Interiors, 151, 223-242.

Melles, M., 1992, Late Quaternary paleoglaciology and paleoceanography at the continental margin of the southern Weddell Sea, Antarctica. Polarstern Abstracts, 6, 128-129.

Meyers, N.C., 1982, Marine geology of the western Ross Sea: implications for Antarctic glacial history. Unpublished MS Thesis, Rice University, https://hdl.handle.net/ 1911/104019.

Meynadier, L., Valet, J.-P., Bassinot, F.C., Shackleton, N.J. and Guyodo, Y., 1994, Asymmetrical saw-tooth pattern of the geomagnetic field intensity from equatorial sediments in the Pacific and Indian Oceans. Earth and Planetary Science Letters, 126, 109-127.

Mudelsee, M. and Schulz, M., 1997, The Mid-Pleistocene climate transition: onset of 100 ka cycle lags ice volume

build-up by 280 ka. Earth and Planetary Science Letters, 151, 117-123.

Nishiizumi, K., Imamura, M., Caffee, M.W., Southon, J.R., Finkel, R.C. and McAninch, J., 2007, Absolute calibration of ^{10}Be AMS standards. Nuclear Instruments and Methods in Physics Research Section B: Beam Interactions with Materials and Atoms, 258, 403-413.

Ohneiser, C., Yoo, K.-C., Albot, O.B., Cortese, G., Riesselman, C., Lee, J.I., McKay, R., Bollen, M., Lee, M.K., Moon, H.S., Kim, S., Beltran, C., Levy, R. and Wilson, G.S., 2019, Magneto-biostratigraphic age models for Pleistocene sedimentary records from the Ross Sea. Global and Planetary Change, 176, 36-49.

Orsi, A.H., Jacobs, S.S., Gordon, A.L. and Visbeck, M., 2001, Cooling and ventilating the abyssal ocean. Geophysical Research Letters, 28, 2923-2926.

Park, J., Kim, H.-C., Jo, Y.-H., Kidwell, A. and Hwang, J., 2018, Multi-temporal variation of the Ross Sea Polynya in response to climate forcings. Polar Research, 37, 1444891.

Pritchard, H.D., Ligtenberg, S.R.M., Fricker, H.A., Vaughan, D.G., van den Broeke, M.R. and Padman, L., 2012, Antarctic ice-sheet loss driven by basal melting of ice shelves. Nature, 484, 502-505.

Pudsey, C.J., 1992, Late Quaternary changes in Antarctic Bottom Water velocity inferred from sediment grain size in the northern Weddell Sea. Marine Geology, 107, 9-33.

Raisbeck, G.M., Yiou, F., Cattani, O. and Jouzel, J., 2006, 10Be evidence for the Matuyama-Brunhes geomagnetic reversal in the EPICA Dome C ice core. Nature, 444, 82-84.

Rhee, H.H., Seong, Y.B., Jeon, Y.G. and Yu, B.Y., 2017, Bouldery slope landforms on Mt. Biseul, Korea, and implications for paleoclimate and slope evolution. Quaternary Research, 88, 293-312.

Ship, S. anderson, J. and Domack, E., 1999, Late Pleistocene-Holocene retreat of the West Antarctic Ice-Sheet system in the Ross Sea: part 1-geophysical results. Geological Society of America Bulletin, 111, 1486-1516.

Simon, Q., Thouveny, N., Bourles, D.L., Nuttin, L., Hillaire-Marcel, C. and St-Onge, G., 2016a, Authigenic ^{10}Be/^{9}Be ratios and ^{10}Be-fluxes (^{230}Th$_{xs}$-normalized) in central Baffin Bay sediments during the last glacial cycle: Paleoenvironmental implications. Quaternary Science Reviews, 140, 142-162.

Simon, Q., Thouveny, N., Bourlès, D.L., Valet, J., Bassinot, F., Ménabréaz, L., Guillou, V., Choy, S. and Beaufort, L., 2016b, Authigenic ^{10}Be/^{9}Be ratio signatures of the cosmogenic nuclide production linked to geomagnetic dipole moment variation since the Brunhes/Matuyama boundary. Journal of Geophysical Research: Solid Earth, 121, 7716-7741.

Simon, Q., Thouveny, N., Bourlès, D.L., Valet, J.-P. and Bassinot, F., 2020, Cosmogenic ^{10}Be production records reveal dynamics of geomagnetic dipole moment (GDM) over the Laschamp excursion (20-60 ka). Earth and Planetary Science Letters, 550, 116547.

Singer, B.S., Hoffman, K.A., Coe, R.S., Brown, L.L., Jicha, B.R., Pringle, M.S. and Chauvin, A., 2005, Structural and temporal requirements for geomagnetic field reversal deduced from lava flows. Nature, 434, 633-636.

Sjunneskog, C., Scherer, R., Aldahan, A. and Possnert, G., 2007, ^{10}Be in glacial marine sediment of the Ross Sea, Antarctica, a potential tracer of depositional environment and sediment chronology. Nuclear Instruments and Methods in Physics Research Section B: Beam Interactions with Materials and Atoms, 259, 576-583.

Snyder, C.W., 2016, Evolution of global temperature over the past two million years. Nature, 538, 226-228.

Suganuma, Y., Okada, M., Horie, K., Kaiden, H., Takehara, M., Senda, R., Kimura, J.-I., Kawamura, K., Haneda, Y., Kazaoka, O. and Head, M.J., 2015, Age of Matuyama-Brunhes boundary constrained by U-Pb zircon dating of a widespread tephra. Geology, 43, 491-494.

Sutter, J., Fischer, H., Grosfeld, K., Karlsson, N.B., Kleiner, T., Van Liefferinge, B. and Eisen, O., 2019, Modelling the Antarctic Ice Sheet across the mid-Pleistocene transition-implications for Oldest Ice. The Cryosphere, 13, 2023-2041.

Taviani, M. and Claps, M., 1998, Biogenic Quaternary carbonates in the CRP-1 drillhole, Victoria Land basin, Antarctica. Terra Antartica, 5, 411-418.

Taviani, M., Reid, D.E. and Anderson, J.B., 1993, Skeletal and isotopic composition and paleoclimatic significance of late Pleistocene carbonates, Ross Sea, Antarctica. Journal of Sedimentary Research, 63, 84-90.

Theissen, K.M., Dunbar, R.B., Cooper, A.K., Mucciarone, D.A. and Hoffmann, D., 2003, The Pleistocene evolution of the East Antarctic Ice Sheet in the Prydz Bay region: stable isotopic evidence from ODP Site 1167. Global and Planetary Change, 39, 227-256.

Thompson, A.F., Stewart, A.L., Spence, P. and Heywood, K.J., 2018, The Antarctic Slope Current in a changing climate. Reviews of Geophysics, 56, 741-770.

Valet, J.-P. and Meynadier, L., 1993, Geomagnetic field intensity and reversals during the past four million years. Nature, 366, 234-238.

von Blanckenburg, F., Bouchez, J., Ibarra, D.E. and Maher, K., 2015, Stable runoff and weathering fluxes into the oceans over Quaternary climate cycles. Nature Geoscience, 8, 538-542.

von Blanckenburg, F., Bouchez, J. and Wittmann, H., 2012, Earth surface erosion and weathering from the ^{10}Be (meteoric)/^{9}Be ratio. Earth and Planetary Science Letters, 351, 295-305.

von Blanckenburg, F., O'nions, R.K., Belshaw, N.S., Gibb, A. and Hein, J.R., 1996, Global distribution of beryllium isotopes in deep ocean water as derived from Fe-Mn crusts. Earth and Planetary Science Letters, 141, 213-226.

von Blanckenburg, F. and Willenbring, J.K., 2014, Cosmogenic nuclides: Dates and rates of Earth-surface change. Elements, 10, 341-346.

Willenbring, J.K. and von Blanckenburg, F., 2010, Meteoric cosmogenic Beryllium-10 adsorbed to river sediment and soil: Applications for Earth-surface dynamics. Earth-Science Reviews, 98, 105-122.

Worm, H.-U., 1997, A link between geomagnetic reversals and events and glaciations. Earth and Planetary Science Letters, 147, 55-67.

Yamazaki, T., 1999, Relative paleointensity of the geomagnetic field during Brunhes Chron recorded in North Pacific deep-sea sediment cores: orbital influence?. Earth and planetary science letters, 169, 23-35.

Yin, Q., 2013, Insolation-induced mid-Brunhes transition in Southern Ocean ventilation and deep-ocean temperature. Nature, 494, 222-225.

Yin, Q.Z. and Berger, A., 2010, Insolation and CO_2 contribution to the interglacial climate before and after the Mid-Brunhes Event. Nature Geoscience, 3, 243-246.

Yokoyama, Y. anderson, J.B., Yamane, M., Simkins, L.M., Miyairi, Y., Yamazaki, T., Koizumi, M., Suga, H., Kusahara, K., Prothro, L., Hasumi, H., Southon, J.R. and Ohkouchi, N., 2016, Widespread collapse of the Ross Ice Shelf during the late Holocene. Proceedings of the National Academy of Sciences, 113, 2354-2359.

Received : June 23, 2021
Revised : July 20, 2021
Accepted : August 3, 2021